PAPER

Rapid area change in pitch-up manoeuvres of small perching birds

To cite this article: D T Polet and D E Rival 2015 *Bioinspir. Biomim.* **10** 066004

IOP Publishing Bioinspir. Biomim. 10 (2015) 066004 doi:10.1088/1748-3190/10/6/066004

Bioinspiration & Biomimetics

RECEIVED
27 February 2015

REVISED
8 September 2015

ACCEPTED FOR PUBLICATION
15 September 2015

PUBLISHED
26 October 2015

PAPER

Rapid area change in pitch-up manoeuvres of small perching birds

D T Polet[1] and D E Rival[1,2]

[1] Department of Mechanical and Manufacturing Engineering, University of Calgary, Calgary, AB T2N 1N4, Canada
[2] Department of Mechanical and Materials Engineering, Queen's University, Kingston, ON K7L 3N6, Canada

E-mail: dtpolet@ucalgary.ca

Keywords: bird flight, perching, micro aerial vehicles, rapid area change, aerodynamics

Supplementary material for this article is available online

Abstract

Rapid pitch-up has been highlighted as a mechanism to generate large lift and drag during landing manoeuvres. However, pitching rates had not been measured previously in perching birds, and so the direct applicability of computations and experiments to observed behaviour was not known. We measure pitch rates in a small, wild bird (the black-capped chickadee; *Poecile atricapillus*), and show that these rates are within the parameter range used in experiments. Pitching rates were characterized by the *shape change number*, a metric comparing the rate of frontal area increase to acceleration. Black-capped chickadees increase the shape change number during perching in direct proportion to their total kinetic and potential energy at the start of the manoeuvre. The linear relationship between dissipated energy and shape change number is in accordance with a simple analytical model developed for two-dimensional pitching and decelerating airfoils. Black-capped chickadees use a wing pitch-up manoeuvre during perching to dissipate energy quickly while maintaining lift and drag through rapid area change. It is suggested that similar pitch-and-decelerate manoeuvres could be used to aid in the controlled, precise landings of small manoeuvrable air vehicles.

1. Introduction

Birds employ a diverse repertoire of unsteady manoeuvres, such as banking, braking, takeoff and landing, to navigate dense habitats and respond to gusts. Micro aerial vehicles (MAVs) are flying machines similar in size to small birds, designed to carry out remote sensing tasks in cluttered airspaces. Mimicking the manoeuvrability of birds, in particular the ability to land safely on small platforms, would allow these vehicles to complete their objectives effectively and efficiently. Though progress has been made in designing perching MAVs (Reich *et al* 2009, Doyle *et al* 2011, Moore *et al* 2014), existing MAVs cannot match the control, precision and speed of natural flyers in landing manoeuvres.

In order to perch, a bird must transition from a cruising speed to a standstill at landing. Perching birds simultaneously adjust their body and wing posture to become more vertical (Carruthers *et al* 2007, Berg and Biewener 2010, Provini *et al* 2014), as a horizontal posture reduces drag during cruising flight while an upright posture facilitates larger angles of attack for deceleration. Carruthers *et al* (2007) noted that a steppe eagle would perform a *rapid pitch-up manoeuvre* during perching sequences, where the angle of attack increased continuously from near-horizontal to near-vertical. However, steady state aerodynamic analysis predicted a loss of lift at high angles of attack, due to stall effects combined with a reduction of airspeed (Carruthers *et al* 2010).

Polet *et al* (2015) showed that a rapidly pitching airfoil can achieve large instantaneous and time-averaged lift and drag, even while decelerating to a stop and pitching to a 90° angle of attack. In that study, the pitch rate was parameterized through the shape change number, Ξ. Forces increased as Ξ^2 through a combination of added-mass energy transfer and vorticity generation. These results suggest that rapid area change through dynamic pitching helps generate the forces required by a perching bird to quickly decelerate and stay aloft.

Though prior works have noted body reorientation and wing pitch-up in perching birds (Carruthers *et al* 2007, Berg and Biewener 2010, Provini *et al* 2014), none have reported wing pitching rates in these birds

or demonstrated that the resulting area change is associated with large forces on the body. We measure pitch rates in the black-capped chickadee (*Poecile atricapillus* Linnaeus 1766), a passerine abundant to North America with an average mass of about 10 g (Chaplin 1974) that will readily approaching feeders at high speeds. These traits—abundance, small size, ease of attraction and speed of approach—make it an ideal candidate for studying high-performance deceleratory manoeuvres with applications to MAVs.

In the present work, we describe fast pitching during perching in the black-capped chickadee, parameterize pitch rates in terms of the shape change number, and show that black-capped chickadees alter their shape change number as the energetic demands of perching increase, implying that rapid area change through dynamic pitching is a kinematic tool that can be tuned to meet the needs of small manoeuvring air vehicles.

2. Energy dissipation through rapid area change

A change in angle of attack increases the frontal area of a wing. This is an example of *rapid area change*, in which an accelerating body exhibits quick expansion or contraction of frontal area. Weymouth and Triantafyllou (2013) showed that rapid area change is characterized by the *shape change number*

$$\Xi = \frac{V^2}{aL}, \tag{1}$$

where V is the outward or inward velocity of area change, a is the body acceleration and L is a body length scale. Weymouth and Triantafyllou (2013) demonstrated that altering the shape change number can dramatically modify the added mass, boundary-layer vorticity and forces on a body.

These arguments were extended by Polet *et al* (2015) to a two-dimensional pitching airfoil decelerating from initial velocity U_0 to a halt. Substitution of kinematic parameters into equation (1) revealed that

$$\Xi = \frac{V}{U_0}, \tag{2}$$

showing that the shape change number in their case compares the change in frontal area relative to a characteristic change in forward velocity. As the metric shown in equation (2) was constructed in two-dimensional space, it requires some modification to be applied to a three-dimensional perching bird. We derive an analogous shape change number in section 4.2, after establishing the characteristic perching behaviour within *P. atricapillus*.

As rapid area change is an effective means to shed energy, we expect a relationship between the shape change number used by birds and the energetic demands of a perching manoeuvre. Once a bird has perched successfully, its kinetic and gravitational potential energy relative to the perch are both zero. The total change in energy is therefore

$$\Delta E = mg\Delta z + \frac{1}{2}mU_0^2, \tag{3}$$

where m is the bird's mass, g is the acceleration due to gravity, Δz is the height of the bird's centre of mass (CoM) relative to the perch and U_0 the initial speed of its CoM. In principle, any amount of energy could be dissipated with the smallest force, given sufficient time. In practice, however, a bird needs to stay airborne until it lands. Slow deceleration requires longer periods of sustained lift, costing metabolic energy. A fast pitch-up quickly dissipates energy through rapid area change while simultaneously producing enough lift to remain airborne.

Some energetic dissipation comes through the legs at touchdown, but the majority is dissipated aerodynamically (Provini *et al* 2014). The total energy absorbed by the legs is limited by risk of injury, and so must be capped at a maximum value. Assuming that energetic absorption of the legs is constant regardless of the total energetic dissipation in perching, then the total energy dissipated aerodynamically grows in proportion to the change in energy of perching according to equation (3).

Polet *et al* (2015) showed that a pitching and decelerating airfoil produces drag as $D \propto \Xi^2$, while the translational distance scaled as $d \propto 1/\Xi$, due to higher rates of deceleration at higher Ξ. The total energy dissipated in such a manoeuvre scales as

$$\Delta E \propto dD \propto \Xi. \tag{4}$$

Therefore, as a first approximation we expect the shape change number used by these small birds to increase linearly with the energetic requirements of perching manoeuvres. Predicting the slope and intercept of the proportionality (4) would require knowledge of the maximum muscular power output and efficiency, moment of inertia about the wing pitch axis and other biological data not available for this species. However, observing the relationship (4) would support the hypothesis that chickadees employ rapid area change through dynamic pitching during perching manoeuvres.

3. Experimental setup

A rectangular enclosure, 3 m long, 1.2 m wide and 1.4 m high was built to encourage birds to approach from a consistent direction (figure 1). Two sheets of white polyethylene were attached to the long sides, and two layers of 2.5 cm hexagonal wire mesh were fixed on the upper surface. A plastic tray feeder was set 0.9 m above the ground in the centre of the enclosure, and filled with commercially available birdseed. The two smaller faces on opposite sides of the enclosure were left open. As Green and Cheng (1998) showed that birds will manoeuvre differently to land on a novel perch, filming began 11 days after the feeder was

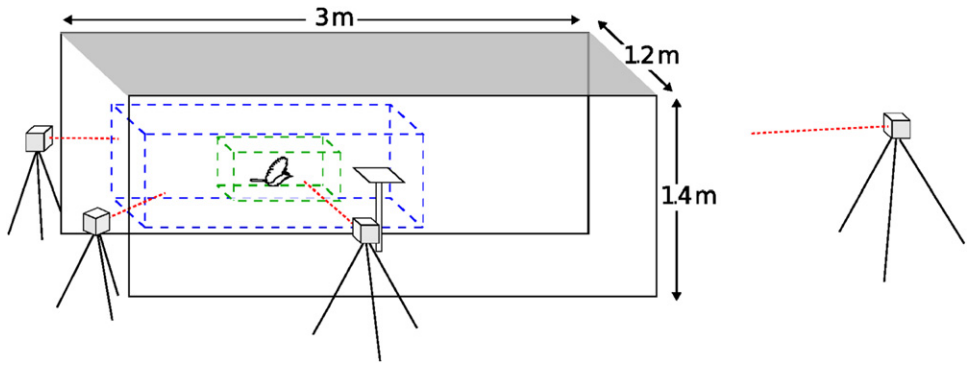

Figure 1. A diagram of the setup used in data collection. A feeder was placed at the centre of an enclosure, which was open at two ends. Four cameras were positioned around the enclosure, forming two reconstruction volumes: a smaller volume for improved resolution of the pitch-up manoeuvre (green) and a larger volume to capture the entire perching sequence (blue).

placed and five days after the enclosure was finished, allowing the birds time to acclimate to the setup.

Four Casio EX-ZR700 high-speed cameras were arranged around the enclosure to allow multiple views of perching sequences. The cameras recorded 224 × 160 pixel colour images at 480 frames per second in 13 min intervals while birds flew to the perch freely. Shutter speed was selected automatically by internal camera software, within the range 1/500-1/10 000 s. Subjects were lit using natural light on sunny days. Camera frame offsets were calculated based on an LED that flashed at the start of each filming sequence. A 10 cm calibration wand was waved through the reconstruction volume, and camera positions were calibrated using the Sparse Bundle Adjustment algorithm packaged in the MATLAB^{TM} script *easyWand5* (Theriault *et al* 2014). The reference frame was aligned to gravity by measuring the acceleration of an object falling through the reconstruction volume. Gravitational acceleration was estimated as 95 ± 5% (mean ± Std) of the expected value of 9.8 m s^{-2}. Calibration reconstruction error was estimated as 1 mm, based on the standard deviation of the wand length for all wand images, and synchronization error was estimated as ±1ms.

Over 30 perching sequences were filmed, however only 11 were deemed acceptable for analysis. The remainder were rejected due to the subject being out of frame in a camera at a critical time, not approaching through the left opening in figure 1, or if irremediable synchronization errors were detected. The acceptable sequences were digitized manually using the MATLAB^{TM} script *DLTdv5*, written by Hedrick (2008). Details of the digitized body parts can be found in figure 2. Averaging across all trials, the direct linear transform root-mean-square error computed by *DLTdv5* was 0.75 pixels for the beak and 1.2 pixels for the wingtip. These are the two points that were respectively the most and least clear in the videos, representing an upper and lower bound on digitization precision. After digitization, position data was processed using custom MATLAB^{TM} scripts. Three-dimensional kinematic position data was smoothed with a second-order low-pass Butterworth filter with 50 Hz cutoff. Velocities and accelerations were computed using two-sided finite difference schemes:

$$\mathbf{u}_i = \left(\mathbf{x}_{i-2} - 8\mathbf{x}_{i-1} + 8\mathbf{x}_{i+1} - \mathbf{x}_{i+2}\right)\Big/(12\Delta t), \quad (5)$$

$$\mathbf{a}_i = \left(-\mathbf{x}_{i-2} + 16\mathbf{x}_{i-1} - 30\mathbf{x}_i + 16\mathbf{x}_{i-1} - \mathbf{x}_{i+2}\right)\Big/\left(12\Delta t^2\right), \quad (6)$$

where $\mathbf{x}$,$\mathbf{u}$ and $\mathbf{a}$ refer to position, velocity and acceleration vectors, respectively, and Δt is the time increment between frames.

The CoM was taken as the average position between the tip of the tail coverts and the base of the beak (figure 2). The tip of the tail coverts was used because it was relatively easy to distinguish in all trials. However, as both tail coverts and head are mobile relative to the CoM, artifacts in acceleration can appear as the bird adjusts its body orientation. To compensate for these artifacts in calculating instantaneous acceleration of the CoM, the true rump location (point 2b in figure 2) was digitized for one trial where it could be distinguished easily. However, movement of the head can still induce artifacts of CoM acceleration, and these will be noted where they appear in the results.

We estimated the bird's initial total energy as described in equation (3). As the mass of each bird was not measured, we assumed a simple geometric scaling of body length to mass ($m \propto \mathcal{L}^3$). To attain the correct units of mass in equation (3), $\mathcal{L}^3$ was multiplied by the arbitrary density 1000 kg m^{-3}, which is considered a reasonable first estimate. Note that the precise density linking length to mass is not required to test the proportionality expressed in equation (4) if $m \propto \mathcal{L}^3$ is assumed. Body length was taken as the mean distance between beak and rump tip from the end of the ballistic phase (t_0; see figure 2 and section 4.1) up to the first complete wrist extension (t_1; figure 2). The birds were all of similar sizes; the average body length was 7 cm, with a range of 1 cm ($N = 11$).

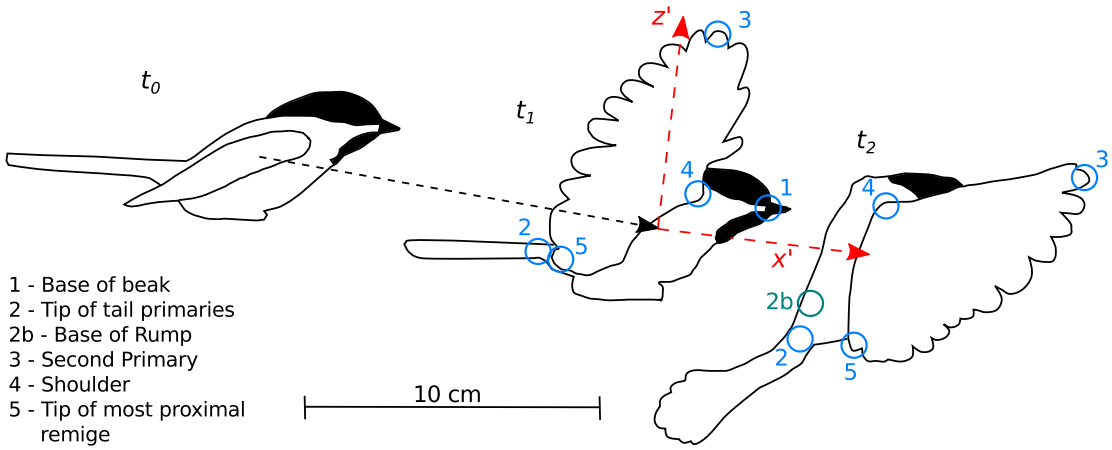

Figure 2. Outlines of a bird extracted from video frames of a single perching sequence, showing (left to right) the end of the ballistic phase (t_0), the first frame where the wrist is fully extended (t_1), and the final frame before the wrist flexes (t_2). The shape change number is calculated between t_1 and t_2. Note the more vertical orientation of both body and wing at t_2 compared to t_1. Digitized points are shown as circles. The angle of attack was measured relative to the plane whose normal is $\mathbf{z}'$, defined as $\mathbf{z}' \equiv \mathbf{x}' \times \mathbf{z} \times \mathbf{x}'$, where $\mathbf{x}'$ denotes the displacement vector of the centre of mass from t_1 to t_2 and $\mathbf{z}$ is the vertical. The time from t_0 to t_1 is 38 ms and time from t_1 to t_2 is 23 ms in this case.

Similarly, U_0 is the average CoM speed from t_0 to t_1. Δz is the height of the CoM relative to the perch at t_1, and g is taken as 9.8 m s^{-2}. Wing length was measured from the wingtip to the shoulder, while the chord is measured from the shoulder to the tip of the most proximal remige (figure 2).

t_2 is taken as the final frame before the wrist flexes following t_1, or, in the single case where the wing tip could not be distinguished up to a minimum of two frames after wrist flexion, as the final frame where velocity could be calculated according to equation (5). The frame rate allowed digitization of 8 time steps on average (minimum of 5, maximum of 13) between t_1 and t_2. The wing was also digitized for a minimum of two additional time steps both before t_1 and after t_2. As the wings appear to be moving symmetrically and yaw is not observed during the manoeuvre of interest (see section 4.2), we measured the kinematics of the right wing only.

The angle of attack was approximated as the wing angle relative to the plane whose normal is $\mathbf{z}'$ (figure 2), defined as $\mathbf{z}' \equiv \mathbf{x}' \times \mathbf{z} \times \mathbf{x}'$, where $\mathbf{x}'$ denotes the displacement vector of the CoM from t_1 to t_2 and $\mathbf{z}$ is the vertical. In the present study, we exclusively use the proximal remige to measure wing angle; however the angle of attack may change along the wing length. Manually digitizing the required number of data points to measure angle of attack across the wing would be impractical, and markers could not be attached to these wild birds without increasing the invasiveness of the study. However, we note that angles of attack along the wing length in pigeons do not differ significantly during any given wing stroke in perching manoeuvres (Berg and Biewener 2010), and assume that the same is true of the black-capped chickadee. Thus, while the angle of attack at the proximal remige may not be the average angle of attack along the wing length, it may act as a first approximation.

4. Results and discussion

Eleven perching sequences were analyzed from two filming sessions five days apart. Based on these sequences, the qualitative perching behaviour of *P. atricapillus* is described in section 4.1. A three-dimensional extension of the two-dimensional shape change number is established in section 4.2. Quantitative kinematic results are presented in section 4.3.

4.1. Overview of perching behaviour in black-capped chickadees

Black-capped chickadees exhibit a *ballistic phase*[3] before beginning deceleration (figure 2; see supplemental video S1 for a representative perching sequence, slowed 16 times). This phase is characterized by the wings folding tightly around the body and the tail being fully closed, with no apparent active force generation. The bird then enters a *deceleration phase*, characterized by changes in wing and tail kinematics as well as body orientation. At the start of this deceleration phase, the wings quickly extend to begin the first forward power stroke. Midway through the first downstroke, the wings pitch up. The body also shifts from a horizontal orientation to a more vertical orientation. The tail feathers open as the body posture becomes more vertical. After the first forward stroke, the bird performs a rearward recovery

[3] Chickadees, being relatively small birds, employ flap-bounding during steady flight, a flight style where flapping and flexed-wing bounding phases alternate (Tobalske *et al* 1999). The *ballistic phase* appears similar to a bounding phase, but is notable as it always occurs immediately prior to the pitch-up manoeuvre in this species.

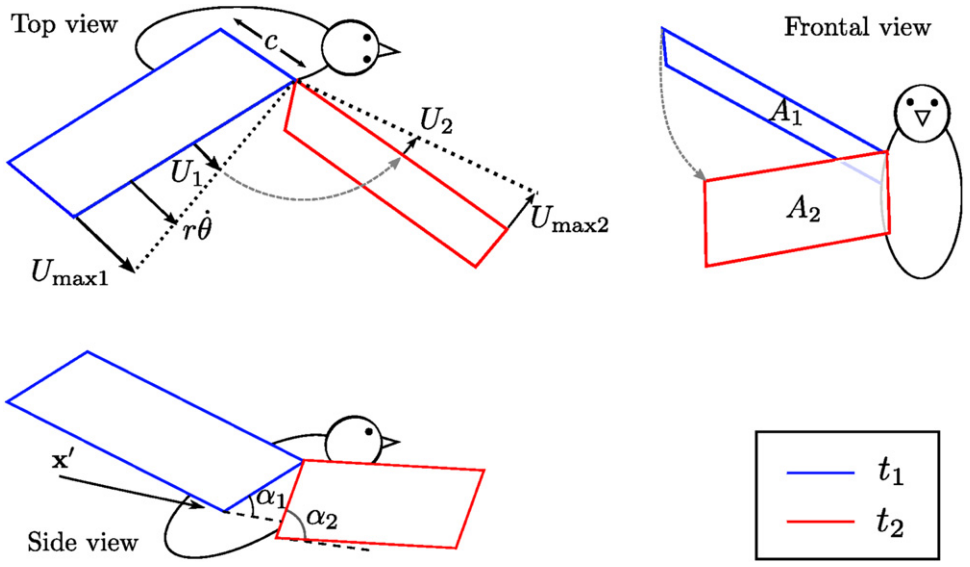

Figure 3. A cartoon showing top, frontal and side views of a bird simultaneously rotating and pitching its wings about the shoulder. Only the right wing is shown in this cartoon. The position of the wing in the bird's frame of reference is shown at t_1 and t_2 (represented by blue and red, respectively), during which time the frontal area of the wing increases.

stroke and begins a sequence of between one and four subsequent power-recovery stroke cycles before touchdown (median 2, mean 2.4, standard error 0.28, $N = 11$).

Power strokes from the wing cause a torque about the bird's CoM, as made evident by the increase in body angle following the first power stroke in the deceleration phase. However, reorientation of the body slows with further forward wing strokes when the tail is fully expanded. This suggests that the tail counteracts the torque produced by the wings while also producing greater drag.

The mean initial flight speed of the chickadees is $3.4 \pm 0.1\ \mathrm{m\,s^{-1}}$, and their landing speed is $1.5 \pm 0.1\ \mathrm{m\,s^{-1}}$ (mean $\pm$ StdErr, $N = 11$). Based on their initial speed and height relative to the perch and speed immediately before touchdown, the birds lose $78 \pm 4\%$ of their total energy aerodynamically (mean $\pm$ StdErr, $N = 11$). This is in contrast to 94% and 96% respectively in the larger zebra finches and diamond doves (Provini *et al* 2014), but is consistent with the notion that smaller animals tend to have more robust legs relative to both their weight and peak locomotory stresses (Biewener 1982). Nevertheless, chickadees dissipate the majority of their energy aerodynamically during perching; thus, aerodynamic mechanisms remain crucial to a successful landing.

In black-capped chickadees, the first downstroke involves a pronounced wing pitch-up manoeuvre, with observed pitch rates ranging between 16 and 39 rads $\mathrm{s^{-1}}$. We therefore analyzed this downstroke in detail using the smaller reconstruction volume (figure 1) to quantify the shape change number and associated forces.

4.2. A three-dimensional analogue to the two-dimensional shape change number

Here we extend the two-dimensional shape change number (Ξ) for a pitching and decelerating airfoil (equation (1)) to an analogous metric relevant to the first perching power stroke described in section 4.1. During the first stroke, there are three ways in which black-capped chickadees can use control surfaces to change frontal area: (1) extending and morphing the wings as they unfold from the body, (2) expanding and pitching the tail and (3) pitching the wings. The latter is most similar to earlier work on two-dimensional pitching airfoils, and so is most amenable to comparative analysis. The first two effects merit future study but are beyond the scope of the present work.

For black-capped chickadees, the majority of wing pitching occurs after the wings are fully extended. From the timestep where the wrist is first extended fully (t_1) to the timestep immediately before the wrist flexes again (t_2; see figure 2), on average the maximum change in wing length is 13% ($\sim$1/8th) of the mean. The small change in wing planform shape fortuitously separates the effects of area change due to pitching from wing expansion. Therefore, Ξ is calculated between t_1 and t_2. The pitch angle to the CoM translation is measured at these two points (α_1 and α_2, respectively; figure 3). We are interested in the area change normal to the chordwise airspeed. Taking the chord length, c, and setting $T = t_2 - t_1$, the shape change velocity is then

$$V = \frac{c\left(\sin\alpha_2 - \sin\alpha_1\right)}{T}. \tag{7}$$

The shape change number requires a characteristic translational velocity change (ΔU). Between t_1 and t_2,

the wing performs a sweeping motion about the shoulder (figure 3). The average chordwise airspeed across the wing is approximately equal to the speed of the wing, normal to its length, at the midpoint between shoulder and wingtip (figure 3). We calculate these airspeeds at t_1 and t_2, producing U_1 and U_2 respectively[4]. As the bird must perform a recovery stroke following t_2, the wings decelerate from t_1 to t_2 while pitching up. Thus, the analogous deceleration to a two-dimensional pitch-and-decelerate manoeuvre is $a = \Delta U/T = (U_2 - U_1)/T$.

Inserting these kinematic values into equation (1) and setting $c = L$, we arrive at

$$\Xi = \frac{V\left[\sin(\alpha_2) - \sin(\alpha_1)\right]}{\Delta U}. \tag{8}$$

Using the same parameters as Polet *et al* (2015) ($\alpha_1 = 0°$, $\alpha_2 = 90°$, $\Delta U = U_0$), we recover equation (2). Thus, equation (8) is analogous to the two-dimensional shape change number for a pitching and decelerating airfoil, and compares the rates of change of frontal width and sweep velocity in a pitching wing.

Note that equation (8) no longer requires a deceleration to a halt, in contrast to equation (2). Therefore, it is not necessarily true that $d \propto 1/\Xi$ and a correction factor must be added to equation (4). Assuming constant deceleration from U_1 to U_2, we can express the distance the wing travels as $d = (U_1 + U_2)T/2$. Using equations (7) and (8), it can be easily shown that

$$d = \frac{U_1 + U_2}{U_1 - U_2}\frac{c\left(\sin\alpha_2 - \sin\alpha_1\right)^2}{2\Xi}. \tag{9}$$

Thus, the relationship between ΔE and Ξ becomes

$$\Delta E \propto \left(\frac{U_1 + U_2}{U_1 - U_2}c\left(\sin\alpha_2 - \sin\alpha_1\right)^2\right)\Xi \equiv \mathcal{C}\Xi, \tag{10}$$

where the symbol $\mathcal{C}$ is given to the correction factor. $\mathcal{C}\Xi$ is proportional to the aerodynamic energetic dissipation from area change through pitching, which we expect to increase along with the energetic demands of a perching manoeuvre.

4.3. Rapid pitch-up manoeuvres and area change to increase force production

Figure 4 shows the instantaneous CoM accelerations due to vertical and rearward forces (roughly lift and drag) for a representative trial. Vertical lines denote t_0, t_1 and t_2 as shown in figure 2. The greatest pitching occurs between t_1 and t_2. A relatively large peak in vertical and rearward acceleration occurs at the onset of the pitch-up manoeuvre. The peak rearward acceleration is followed by a peak forward acceleration. Since the CoM is defined as the average position of beak and rump, the peak forward acceleration is likely an artifact of the forward rotation of the head relative to the body (figure 2). This same rotation would also detract from the observed magnitudes of rearward acceleration; thus, despite these artifacts figure 4 shows that the largest drag produced between t_0 to t_2 occurs during the pitch-up manoeuvre when the wrists are fully extended.

Figure 5(a) plots the shape change number according to equation (8) for individual perching sequences against each bird's total potential and kinetic energy relative to the perch at t_0. Shape change number varies from 0.01 to 0.20, within the range tested by Polet *et al* (2015). Shape change number increases with initial kinematic energy, supporting the hypothesis that pitch rates are tuned by small birds to the energetic demands of the perching manoeuvre. Using all trials, the R^2 value of the linear least-squares fit is 0.54 ($p = 0.01$). Of note is a single trial, denoted by a circle in figure 5, which exhibits a much higher shape change number given its initial energy as compared to the others. In this sequence, unlike the others, the bird slowed to a near halt before landing, and required an extra lunge near the perch to achieve touchdown (see supplementary video S2). It may be that this individual overestimated its energy requirements and used a higher shape change number than needed to land smoothly. Excluding this outlier, the R^2 value is 0.73 ($p = 0.002$), supporting the relationship developed in equation (4).

In section 4.2, it was noted that the new three-dimensional shape change metric does not necessarily require $d \propto 1/\Xi$, and so a correction factor $\mathcal{C}$ is necessary in the relationship between energetic dissipation from area change and total energy change in perching. The shape change number multiplied by this correction factor is plotted against energy change in figure 5(b). The trend remains linear overall, but with greater scatter about central tendency. Excluding the outlier as before, the R^2 value is 0.59 ($p = 0.01$).

It may seem that spurious correlations between ΔE and Ξ would arise due to the CoM speed U_0 being a component of the wing velocities U_1 and U_2, as the former term appears in ΔE and the latter two terms in Ξ. However, if $U_0 \propto U_1 - U_2$, we would expect a reciprocal relationship in figure 5(a) in the absence of a physical mechanism linking Ξ and ΔE. As a positive linear trend is observed instead, we conclude that the proposed physical mechanism is indeed responsible.

For $\mathcal{C}\Xi$ versus ΔE, a spurious correlation may arise if $U_1 + U_2$ is proportional to U_0 and $U_1 - U_2$ is not. We therefore tested a linear model on $\mathcal{C}\Xi/(U_1 + U_2)$ versus ΔE, eliminating $U_1 + U_2$ in the response variable, and found $R^2 = 0.65$ and $p = 0.005$ ($N = 10$). Thus, it is unlikely that the dependence of $U_1 + U_2$ on U_0 is responsible for the correlation observed between $\mathcal{C}\Xi$ and ΔE, and rather that the correlation arises because energetic dissipation due to pitch-up is proportional to total energy change during perching.

[4] Based on the average values of $\bar{c} = 0.04$ m and $\bar{U}_1 = 5.9$ m s^{-1}, the Reynolds number in these perching sequences is approximately 2.4×10^4, similar to the value of 2.2×10^4 used by Polet *et al* (2015).

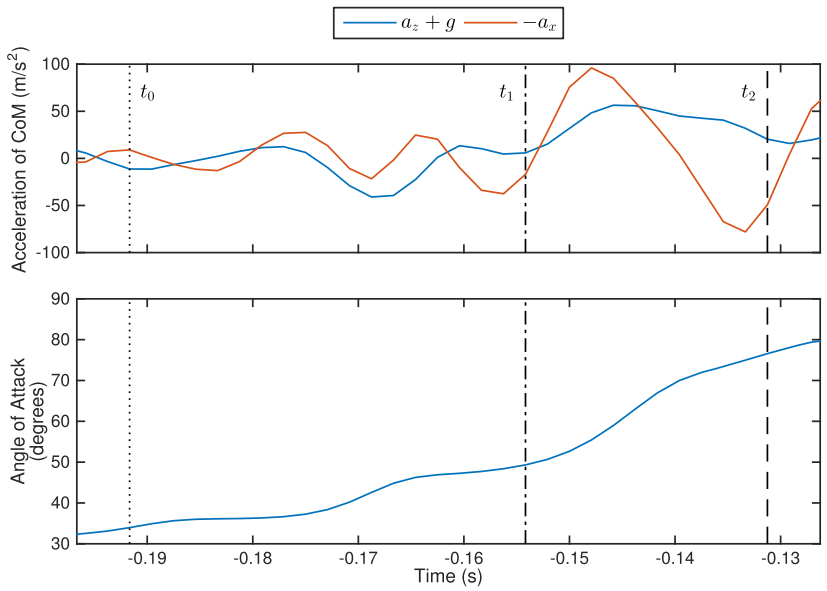

Figure 4. A representative trial, showing that black-capped chickadees exhibit relatively large centre-of-mass (CoM) accelerations along with a rapid increase in angle of attack from the first moment when the wing wrist is fully extended (t_1) to the moment where it is flexed once again (t_2). As the CoM is measured as the midpoint of beak and rump, the peak forward acceleration near the point of arm flexion is likely an artifact due to the head remaining level while the body posture becomes more vertical (figure 2).

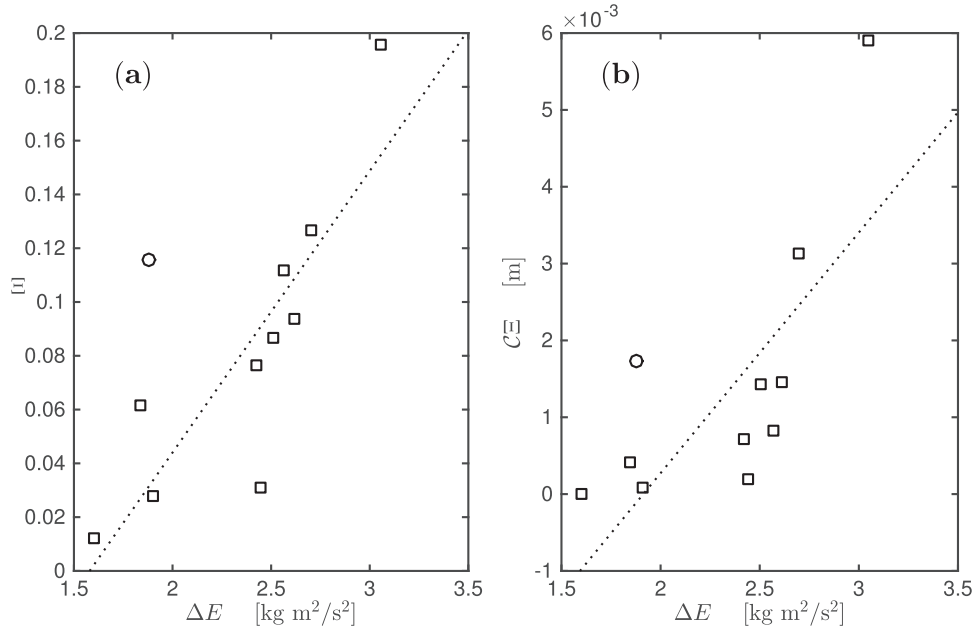

Figure 5. Black-capped chickadees choose higher shape change numbers from wing pitching as the total energetic requirements of the perching manoeuvre increase. (a) The linear trend observed here is consistent with predictions based on pitching and decelerating airfoils (Polet *et al* 2015), without corrections for distance travelled (section 4.2). In the trial denoted with a circle, the bird exhibited an atypical landing pattern as described in the text. Excluding this outlier, the least-squares residual is shown as a dotted line ($R^2 = 0.73$, $p = 0.002$). (b) Here the shape change number is multiplied by a correction factor $\mathcal{C}$ for the new three-dimensional metric (equation (10)), and increases with energetic dissipation ($R^2 = 0.59$; $p = 0.01$).

Because no specimens were captured and marked, and morphological differences between individual chickadees are slight, we could not determine if the same individuals were filmed multiple times. For the present study, we assume that individual biases were minor, and note that the twofold range of ΔE and tenfold range of Ξ provides sufficient variation to test the dependence of shape change number on energetic dissipation in this sample. A future study could capture and mark individuals to test if individual preferences play an important role in the strategies employed; however, such a study would be more invasive.

In section 2 it was assumed that energetic absorption from the legs would be constant regardless of total

energy change in perching. In reality, birds may reduce loading in the legs for less energetic perching manoeuvres, and gradually increase the loading for more energetic manoeuvres up to a particular limit determined by risk of injury. At this point, any additional energy change is exclusively absorbed aerodynamically. Accordingly, in figure 5(b) the energetic dissipation through area change ($\mathcal{C}\Xi$) increases slowly as the total energy change during perching (ΔE) increases, up to approximately $\Delta E = 2.5$ J, at which point further increase in the energy change results in a substantial increase in the energetic dissipation from area change ($\mathcal{C}\Xi$). A follow-up study could use a perch with a built-in force transducer, as used by Bonser and Rayner (1996) and Provini *et al* (2014), to see how energy absorption through perch collision changes with the energetics of a perching manoeuvre.

Birds smaller than 30 g with short, rounded wings seldom glide, and must instead flap frequently to remain airborne (Tobalske 2007). Accordingly, black-capped chickadees perform a rapid pitch-up manoeuvre during a power stroke, rather than during a glide as observed in a steppe eagle (Carruthers *et al* 2007). Performing wing pitch-up at the beginning of the deceleration phase begins the transition to the correct posture for landing while dissipating a large amount of energy. This facilitates slower speeds as the bird approaches the perch and precise control becomes critical, enabling these birds to decelerate on average from 47 body lengths per second to a halt in less than 0.3 s.

The acceleration artifacts from head rotation in this dataset prohibits direct comparison of shape change number and instantaneous acceleration during the pitch-up manoeuvre. Future work could achieve better CoM estimates using markers on captive birds, but this is not an option for wild specimens. While figure 5 shows a strong relationship between shape change number and energetic demands, the exact nature of this relationship should be taken cautiously. Mass could only be estimated as a proportion to length raised to the third power and could not be measured directly. Future studies could implement a weigh scale into the perch itself, enabling accurate measurements of mass once the bird has landed. This would then allow a more precise measure of the exact relationship between area change and energetic demands.

The relationship between pitch rates and energetic dissipation demonstrated in figure 5 suggests a simple, first-order algorithm that could be employed by MAVs during perching manoeuvres: (1) determine the required energy to be dissipated before landing, (2) employ a pitch-up manoeuvre where the shape change number is in proportion to this energy. The slope and intercept of this relationship may well depend on particulars of the shape and size of the aircraft employed. However, the linear relationship between shape change number and energetic dissipation suggests that the slope could be easily calibrated, and the appropriate pitch speed could be readily retrieved during actual perching manoeuvres.

The large peak in lift and drag at the onset of pitching and the choice of larger shape change numbers for more energetic perching manoeuvres support the hypothesis that black-capped chickadees use rapid area change through dynamic pitching to generate large forces for a successful landing. Though high angles of attack can be associated with a loss of lift and control in steady-state flight, black-capped chickadees appear to use a rapid pitch-up manoeuvre—and thus unsteady aerodynamic trickery—to dissipate large amounts of energy dynamically.

5. Conclusions

Birds must be able to dissipate a large amount of energy during landing, but slow deceleration demands longer periods of sustained lift, costing metabolic energy. Rapid pitch-up manoeuvres have been linked to rapid energy dissipation in laboratory experiments on perching airfoils, but pitch rates had not been measured for these manoeuvres in birds. We observed that black-capped chickadees perform a pitch-up manoeuvre during the first deceleratory stroke. This initiates transition to the correct landing posture while also generating large lift and drag. Pitching rates during this power stroke were characterized by the *shape change number*, a metric comparing the rate of frontal area increase to wing acceleration. The shape change number was constructed to be appropriate for the manoeuvres employed by black-capped chickadees while being analogous to the parameter used by Polet *et al* (2015), who revealed that forces increase quadratically with the shape change number in a perching airfoil. We expected and observed black-capped chickadees to choose larger shape change numbers as the energetic demands of the manoeuvre increased. The relationship between shape change number and the total energy change in perching is generally linear, in accordance with simple analytical arguments. These small birds employ rapid-area change through pitching to enable extraordinary manoeuvrability.

Acknowledgments

The authors wish to thank the Natural Sciences and Engineering Research Council of Canada and Alberta Innovates Technology Futures for financial support.

References

Berg A M and Biewener A A 2010 Wing and body kinematics of takeoff and landing flight in the pigeon (*Columba livia*) *J. Exp. Biol.* **213** 1651–8

Biewener A A 1982 Bone strength in small mammals and bipedal birds: do safety factors change with body size? *J. Exp. Biol.* **98** 289–301

Bonser R H C and Rayner J M V 1996 Measuring leg thrust forces in the common starling *J. Exp. Biol.* **199** 435–9

Carruthers A C, Thomas A L R and Taylor G K 2007 Automatic aeroelastic devices in the wings of a steppe eagle *Aquila nipalensis J. Exp. Biol.* **210** 4136–49

Carruthers A C, Thomas A L R, Walker S M and Taylor G K 2010 Mechanics and aerodynamics of perching manoeuvres in a large bird of prey *Aeronaut. J.* **114** 673–80

Chaplin S B 1974 Daily energetics of the black-capped chickadee *Parus atricapillus*, in winter *J. Comp. Physiol.* **89** 321–30

Doyle C E, Bird J J, Isom T A, Johnson C J, Kallman J C, Simpson J A, King R J, Abbott J J and Minor M A 2011 Avian-inspired passive perching mechanism for robotic rotorcraft *2011 IEEE/RSJ Int. Conf. on Intelligent Robots and Systems* (*IROS*) pp 4975–4980

Green P R and Cheng P 1998 Variation in kinematics and dynamics of the landing flights of pigeons on a novel perch *J. Exp. Biol.* **201** 3309–16

Hedrick T L 2008 Software techniques for two-and three-dimensional kinematic measurements of biological and biomimetic systems *Bioinspiration Biomimetics* **3** 034001

Moore J, Cory R and Tedrake R 2014 Robust post-stall perching with a simple fixed-wing glider using LQR-trees *Bioinspiration Biomimetics* **9** 025013

Polet D T, Rival D E and Weymouth G D 2015 Unsteady dynamics of rapid perching manoeuvres *J. Fluid Mech.* **767** 323–41

Provini P, Tobalske B W, Crandell K E and Abourachid A 2014 Transition from wing to leg forces during landing in birds *J. Exp. Biol.* **217** 2659–66

Reich G W, Wojnar O and Albertani R 2009 Aerodynamic performance of a notional perching MAV design *47th AIAA Aerospace Sciences Meeting* (Reston, VA: American Institute of Aeronautics and Astronautics) (doi:10.2514/6.2009-63)

Theriault D H, Fuller N W, Jackson B E, Bluhm E, Evangelista D, Wu Z, Betke M and Hedrick T L 2014 A protocol and calibration method for accurate multi-camera field videography *J. Exp. Biol.* **217** 1843–8

Tobalske B, Peacock W and Dial K 1999 Kinematics of flap-bounding flight in the zebra finch over a wide range of speeds *J. Exp. Biol.* **202** 1725–39

Tobalske B W 2007 Biomechanics of bird flight *J. Exp. Biol.* **210** 3135–46

Weymouth G D and Triantafyllou M S 2013 Ultra-fast escape of a deformable jet-propelled body *J. Fluid Mech.* **721** 367–85